J Ther Eng, Vol. 9, No. 2, pp. 260–278, March 2023

Journal of Thermal Engineering
Web page info: https://jten.yildiz.edu.tr
DOI: 10.18186/thermal.1272395

Journal of Thermal Engineering

Research Article

Enhanced performance of a microchannel with rectangular vortex generators

Alişan GÖNÜL[1]*, Abdulkerim OKBAZ[2,3]

[1]Department of Mechanical Engineering, Siirt University, Siirt, 56100, Türkiye
[2]Department of Mechanical Engineering, Dogus University, Istanbul, 34722, Türkiye
[3]School of Materials Science and Engineering, Georgia Institute of Technology, Atlanta, GA, 30332, USA

ARTICLE INFO

Article history
Received: 07 December 2022
Accepted: 26 February 2023

Keywords:
Flow Control; Genetic Algorithm; Heat Transfer Enhancement; Microchannel; Vortex Generators

ABSTRACT

Microchannel heat sinks and heat exchangers are widely used in the cooling of electronic systems. However, it is still important to enhance the heat transfer in the microchannel so that the intense heat generated can be removed. Vortex generators (VGs) create secondary flow structures in the flow, increasing the fluid mixing, thinning the thermal boundary layer, and ultimately boosting heat transfer. Here, we have controlled the flow structure and improved the heat transfer with the lowest possible pressure loss by placing VGs of different sizes, numbers, and angles of attack in a microchannel. The improvement in heat transfer is accelerated as vortex intensity increases. The angle of attack has a significant impact on vortex formation lengths, which reach high dimensions around 90°. Furthermore, increasing the VG length significantly increases the vortex formation lengths. The number of VG pairs has a significant impact on heat transfer and pressure losses. As the number of VG pairs increases, so does the area occupied by the secondary flow regions in the microchannel, increasing the fluid mixture and boosting heat transfer. The highest enhancement in heat transfer using VGs is obtained at around 230%, while the corresponding increase in pressure loss is 950%. According to the *JF* factor which we consider a performance evaluation criteria, the best result is around 1.38. The Genetic Aggregation Response Surface Methodology has been applied to numerical results. The related method is realized to produce results that are consistent with the numerical results within a ±5% error interval. All the input parameters considered in the sensitivity analysis have an impact of at least 10% on the output parameters.

Cite this article as: Gönül A, Okbaz A. Enhanced performance of a microchannel with rectangular vortex generators. J Ther Eng 2023;9(2):260–278.

***Corresponding author.**
*E-mail address: alisan.gonul@siirt.edu.tr

This paper was recommended for publication in revised form by Regional Editor Ahmet Selim Dalkilic

Published by Yıldız Technical University Press, İstanbul, Turkey

INTRODUCTION

The rapid advancements of electronic devices, the shrinking of chip sizes, the rapid increase in performance, and the increase in processor speeds with the development of computer technologies have also increased the heat density generated by these devices. The increase in heat generation intensity has also necessitated the development of appropriate thermal management mechanisms for these devices to operate properly. The development of micro-manufacturing methods has paved the way for the development of heat transfer enhancement methods. First, Tuckerman and Pease [1] demonstrated that chips could be effectively cooled by opening microchannels on the circuit board where they are mounted. However, due to narrower channels, pressure drops per unit length also increased considerably. As a result of comparison with various experimental results, it has been proved that the flow in the microchannel can be predicted by conventional Navier-Stokes equations [2]. Consequently, numerous researchers employed experimental [3–12] and numerical methods [12-28] to examine the flow structure and heat transfer phenomena in various types of microchannels.

Microchannels have higher heat transfer than conventional channels, but on the other hand, various heat transfer enhancement methods have been applied in microchannels for more efficient cooling of electronic devices [30–32]. One of them is the vortex generator (VG), which was primarily used in conventional ducts or channels [33–39] and heat exchangers [40–44]. VGs can provide higher heat transfer enhancement and lower corresponding pressure loss compared to turbulators [45]. In contrast to wavy [46], corrugated [47], and louvered fins [48–51], VGs [45,52] increase the fluid mixing and temperature gradient normal to the wall and subsequently increase the convective heat transfer by forming secondary flow structures such as vortices in the flow without changing the direction of the main flow. By inserting VGs of varied numbers and angles into a microchannel, heat transfer can be significantly enhanced. Rectangular VGs implemented in a microchannel decreased the critical Reynolds number, which accelerated the onset of turbulence [53,54]. Similarly, the impact of rectangular VGs positioned in a microchannel on flow and heat transfer was studied numerically by considering the thermophysical fluid properties depending on temperature [55]. Fluid mixing in a T-shaped microchannel via diffusion and convection was significantly enhanced by adding rectangular winglet pairs type VGs [56]. In addition to these, VGs of different shapes, for example, cylindrical-type VGs with quarter-circle and half-circle cross-sections, were employed in a microchannel [57].

In order to increase the heat transfer capacity of microchannels, VG designs should be done properly, and pressure losses should be taken into account to reduce energy consumption as well as heat transfer enhancements. Thus, the highest heat transfer capacity will be achieved with the least possible pressure loss. However, the optimal design may differ depending on the channel type, boundary conditions, or operating conditions. Here, we have used the computational fluid dynamics (CFD) method to predict the flow and heat transfer characteristics of a microchannel with rectangular VGs. The objective of the research is to control the flow structure, maximize heat transfer, and minimize pressure loss by varying the relevant parameters. Using response surface methods with genetic algorithm, we have asserted the optimum design of VGs and determined the effects of design and operating parameters. We believe that this study will shed light on the heat transfer enhancement with VGs and guide thermal management engineers in the design of cooling systems.

THEORY

Physical and numerical models

The microchannel with rectangular VGs is depicted in Fig. 1 as a schematic. Dimensionally, the microchannel is 20000 mm in length, 1500 mm in width, and 100 mm in height, with a 1000 mm gap from the channel inlet to the first set of VGs pairs (L_1).

As presented in Fig. 1, L_{VG}, S_{VG} and W_1 represent VG height, the longitudinal pitch of VG pairs and the transverse pitch of VGs in VG pairs, respectively. In addition, the value of S_{VG} indicates the longitudinal distance between VG pairs. Five distinct row numbers (three, four, five, six, and seven) of the VG pairs are studied in this investigation, and five sequential VG pairs put in the microchannel are presented in Fig. 1. Besides, α_1 and α_2 depict the attack angles of two different rectangular VGs layouts (see Fig. 1). Here, we have conducted numerical analysis for different fluid velocities, attack angles, the transverse pitch between VGs in a pair, number of VG pairs, and VG length. Table 1 demonstrates the considered ranges of geometrical parameters employed in response surface methodology and sensitivity analysis. Besides, the VGs have a fixed width of 40 mm.

The ANSYS Fluent 19.1 is utilized to solve three dimensional-turbulent flow and heat transfer domain in the microchannel. Since heat transfer in a microchannel with VGs relies on the conjugate heat transfer mechanism, the energy equations for both solid domain conduction and convection between solid and fluid zones are solved. The time average of the transport and governing equations yields the RANS equations. In steady-state conditions, continuity, momentum, and energy equations for fluid and solid zones are as below, respectively:

$$\frac{\partial u_i}{\partial x_j} = 0 \tag{1}$$

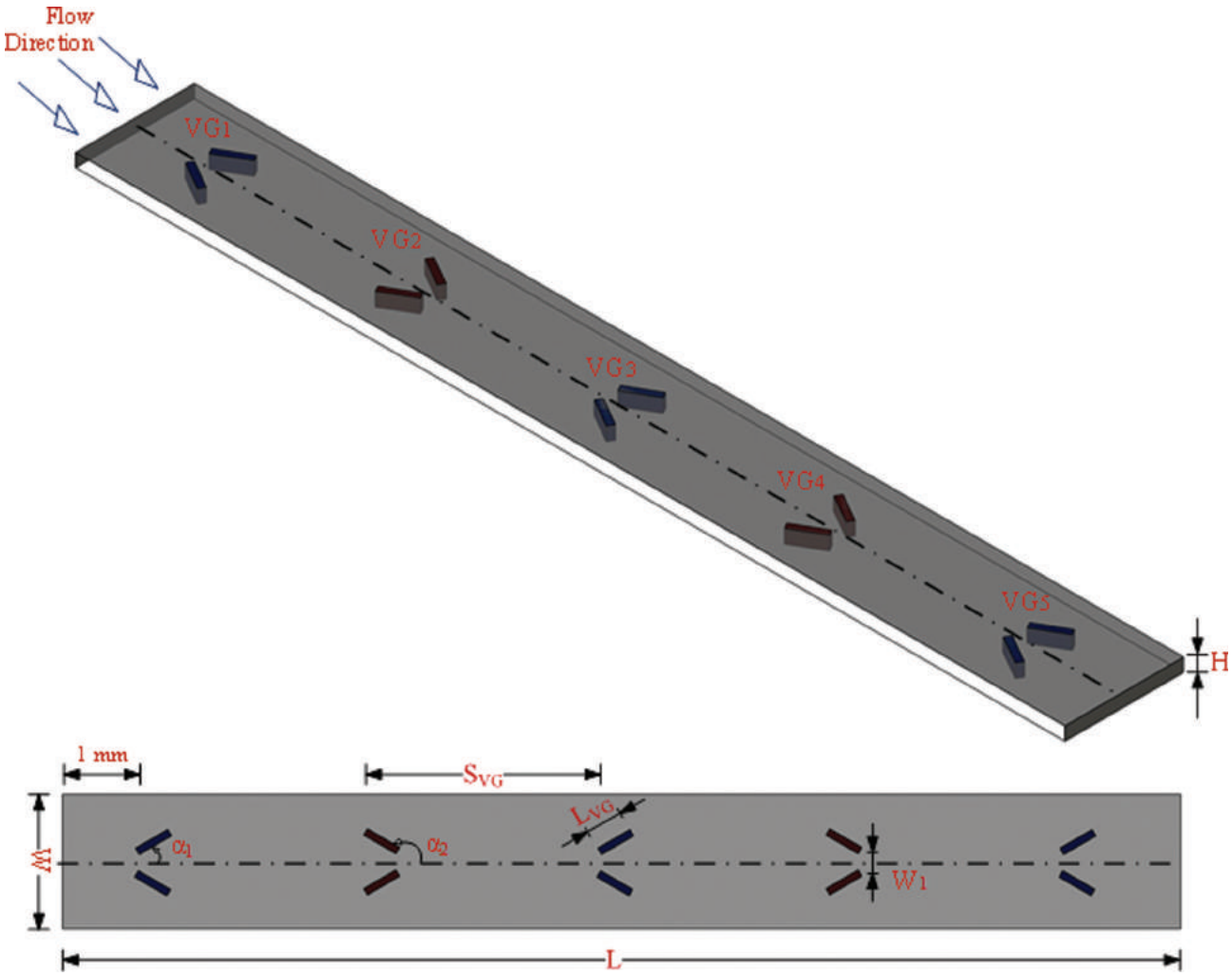

Figure 1. Physical model.

Table 1. The considered range of input parameters

Geometrical parameters	Considered ranges
Flow velocity, V_f(m/s)	3-10
VG length, L_{VG} (μm)	175-500
VG number, N_{VG}	3-7
The transverse pitch between VGs in a pair, W_1 (μm)	70-400
The angle of attack, α_1 (°)	0 < α < 180
The angle of attack, α_2 (°)	0 < α < 180

$$\frac{\partial\left(u_i u_j\right)}{\partial x_j}=-\frac{1}{\rho}\frac{\partial P}{\partial x_i}+\frac{\partial}{\partial x_j}\left[v\left(\frac{\partial u_i}{\partial x_j}+\frac{\partial u_j}{\partial x_i}-\frac{2}{3}\delta_{ij}\frac{\partial u_j}{\partial x_j}\right)\right]+\frac{\partial}{\partial x_j}\left(-\overline{u_i' u_j'}\right) \quad (2)$$

Where u_i and p are time or ensemble average component, u_i' are the fluctuating components. $\left(-\overline{u_i' u_j'}\right)$ represents the effect of turbulence and is known as the Reynolds stress tensor. It is defined as below;

$$-\overline{u_i' u_j'}=v_t\left(\frac{\partial u_i}{\partial x_j}+\frac{\partial u_j}{\partial x_i}\right)-\left(\frac{2}{3}k+v_t\frac{\partial u_k}{\partial x_k}\right)\delta_{ij} \quad (3)$$

The Reynolds-averaged method for simulating turbulence requires that the Reynolds stresses in Eq. 2 be accurately modeled. A common method for determining the relationship between Reynolds stresses and mean velocity gradients uses the Boussinesq hypothesis [60,61]. In ANSYS Fluent, turbulent heat transport is modeled employing the concept of the Reynolds analogy to turbulent momentum transfer. The modeled energy equation for fluid domain is given as below:

$$\frac{\partial}{\partial x_i}\left[u_i\left(E+\frac{p}{\rho}\right)\right]=\frac{1}{\rho}\frac{\partial}{\partial x_i}\left[\left(\lambda+\frac{c_p\mu_t}{\mathrm{Pr}_t}\right)\frac{\partial T}{\partial x_i}\right] \quad (4)$$

In Eq. 4, E is the total energy per unit mass consisting of internal, kinetic, and potential energies ($E = c_v T + u^2/2$, the potential energy is omitted). Also, Pr_t is the turbulent Prandtl number. The energy equation for solid domain:

$$\lambda_s\frac{\partial^2 T}{\partial x_j^2}=0 \quad (5)$$

SST k-ω turbulence model has some advantages over the Standard form of k-ω and k-ε turbulence models, and it generally increases the accuracy of the model for predicting free shear flows. In this model, the cross-diffusion term and mixing function in the ω equation can provide better results in the near-wall and far-field regions. The transport equation of this model is as follows:

$$\frac{\partial(\rho k u_i)}{\partial x_i}=\frac{\partial}{\partial x_i}\left[\Gamma_k\frac{\partial k}{\partial x_i}\right]+G_k-Y_k \quad (6)$$

$$\frac{\partial(\rho\omega u_i)}{\partial x_i}=\frac{\partial}{\partial x_i}\left[\Gamma_k\frac{\partial \omega}{\partial x_i}\right]+G_\omega+D_\omega-Y_\omega \quad (7)$$

In these equations, G_k denotes the production of kinetic energy due to turbulence. G_ω symbolizes the generation of ω. Γ_k and Γ_ω denote the effective diffusivities of k and ω, while Y_k and Y_ω symbolize the dissipation of k and ω due to turbulence. D_ω represents the term for cross-diffusion. User-defined source terms are omitted from the modeling as they are not utilized. Ref. [60] can be examined for information on the associated turbulence model.

The velocity inlet boundary condition is implemented at the inlet, while the pressure boundary condition is performed at the outlet (0 Pa gauge pressure). In order to eliminate entrance and exit influences, the slip wall boundary condition is implemented at the flow domain walls positioned at $20D_h$ and $40D_h$ from the inlet and outlet, respectively. In contrast, the no-slip boundary condition is implemented on the walls of the test domain. The symmetry boundary condition is used at the middle of in the microchannel to reduce the solution cost. The constant surface temperature (323.15 K) is applied to the bottom wall of the test domain. Silicon and deionized water are utilized as the coolant fluid and VG material, respectively. The thermophysical properties of silicon and deionized water as a function of temperature are listed in Table 2.

The pressure-based solver is utilized while the coupled algorithm is preferred for velocity-pressure coupling. Spatial discretization for governing equations is realized by a second-order upwind scheme. The least squares gradient is used for better accuracy considering mesh imperfections in terms of orthogonality. It is confirmed that the residuals of the continuity, momentum and energy equations are less than 10^{-5}, 10^{-7}, and 10^{-9}, respectively. Fig.2 depicts the applied boundary conditions and the created mesh details on flow and solid domains.

Table 2. Silicon and deionized water thermophysical properties [58,59]

Properties	Silicon	Deionized-water
ρ (kg.m^{-3})	2330	998.2
k (W.m^{-2}.K^{-1})	290+0.4T	$-0.829 + 0.0079T - 1.04 \times 10^{-5}T^2$
C_p (J.kg^{-2}.K^{-1})	390+0.9T	$5348 - 7.42T + 1.17 \times 10^{-2}T^2$
μ (Pa.s)	---	$0.0194 - 1.065 \times 10^{4}T + 1.489 \times 10^{-7}T^2$

Some parameters are offered below to determine the thermal and flow performances of microchannels with VGs. The Reynolds number is determined as follows:

$$Re=\frac{\rho V_f D_h}{\mu} \quad (8)$$

where D_h is the hydraulic diameter, and it is calculated as follows:

$$D_h=\frac{4A_c}{P_w}=\frac{2WH}{(W+H)} \quad (9)$$

The dimensionless average Nu, a key indicator of heat transfer performance, is defined as follows:

$$Nu=\frac{hD_h}{k_f} \quad (10)$$

where h indicates the average heat convection coefficient, and it is calculated as follows:

$$h=\frac{\dot{Q}}{A_h\Delta T_m} \quad (11)$$

where $\dot{Q}$, A_h, and ΔT_m signify the heat transfer rate, heat transfer surface area (base area), and logarithmic mean temperature difference (LMTD), respectively. LMTD is described as follows:

$$\Delta T_m=\frac{(T_h-T_i)-(T_h-T_o)}{In\left(\frac{T_h-T_i}{T_h-T_o}\right)} \quad (12)$$

JF, which indicates the relationship in both pressure loss and heat transfer with and without VGs, is

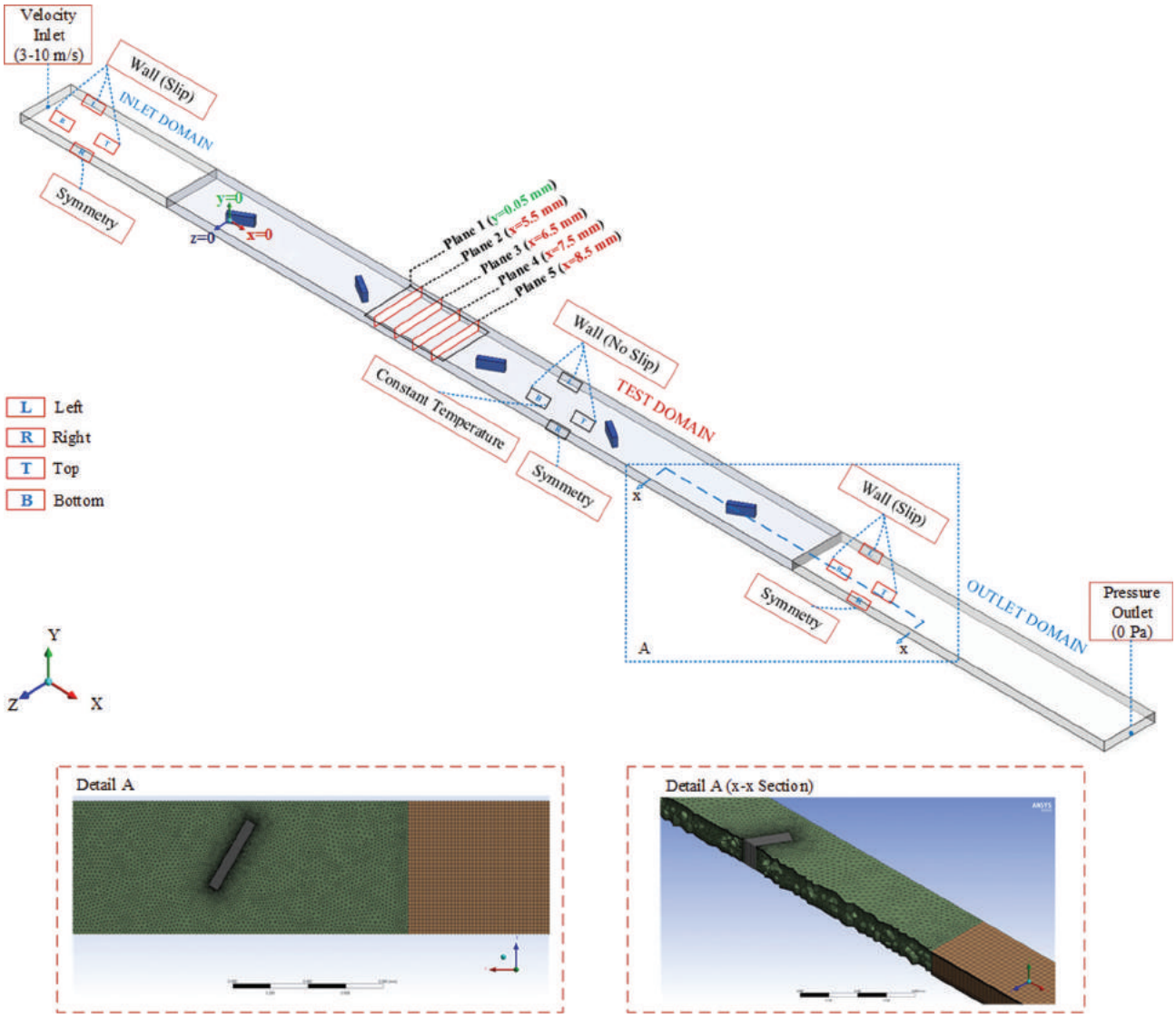

Figure 2. Boundary conditions and mesh detail of computational domain.

utilized to more accurately represent the thermal-hydraulic performance.

$$JF = \frac{j/j_o}{\left(f/f_o\right)^{1/3}} \tag{13}$$

Mesh independency and validation of the numerical model

Based on the experimental findings of Liu et al. [53] four turbulence models (k-ε Realizable EWT, k-ε RNG EWT, k-ω SST, and Reynolds Stress EWT) are used to solve 3D thermal-hydraulic behaviors in microchannels with VGs. Initially, mesh independence of the solution is evaluated for all turbulence models evaluating *Nu* and *f* values (Fig. 3).

The solutions obtained with 2.3 million and 11 million elements differ by approximately 0.2% in both *Nu* and *f* values. Considering this situation and staying in the safe zone, the model with the number of 4.2 million elements has been used in all analyzes.

Fig. 4 depicts the results of the numerical analysis performed in the experimental investigation of Ref. [53], taking into account all specifications of the "G1" channel configuration. The channel's dimensions and characteristics under consideration such as the length, width, the angle of attack, and number of L_{VG} pairs are 400 μm, 50 μm, 30°, and 5, respectively. Fig. 4a and 4b depict comparison of numerical and experimental results for *Nu* and *f* values, respectively. The numerical results for various Reynolds numbers are in strong agreement with the results of the experiments. The maximum deviations between numerical and experimental

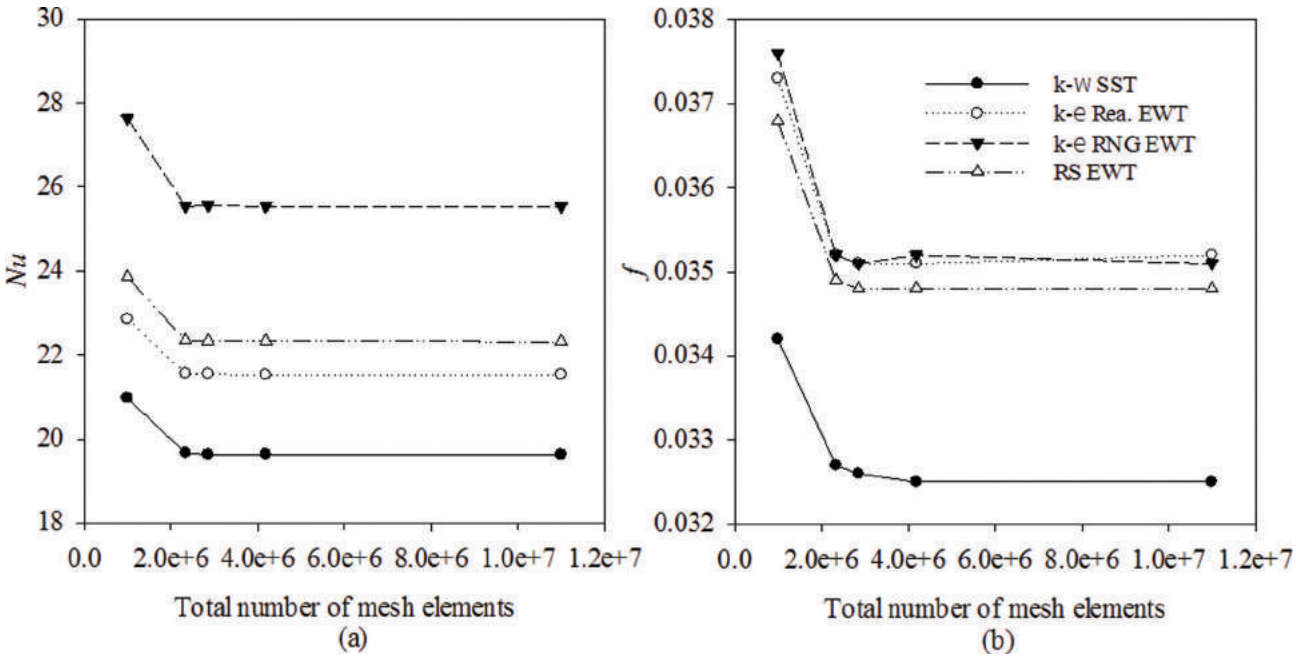

Figure 3. Mesh Independence Studies for Microchannel with VGs **(a)** *Nu*, **(b)** *f*.

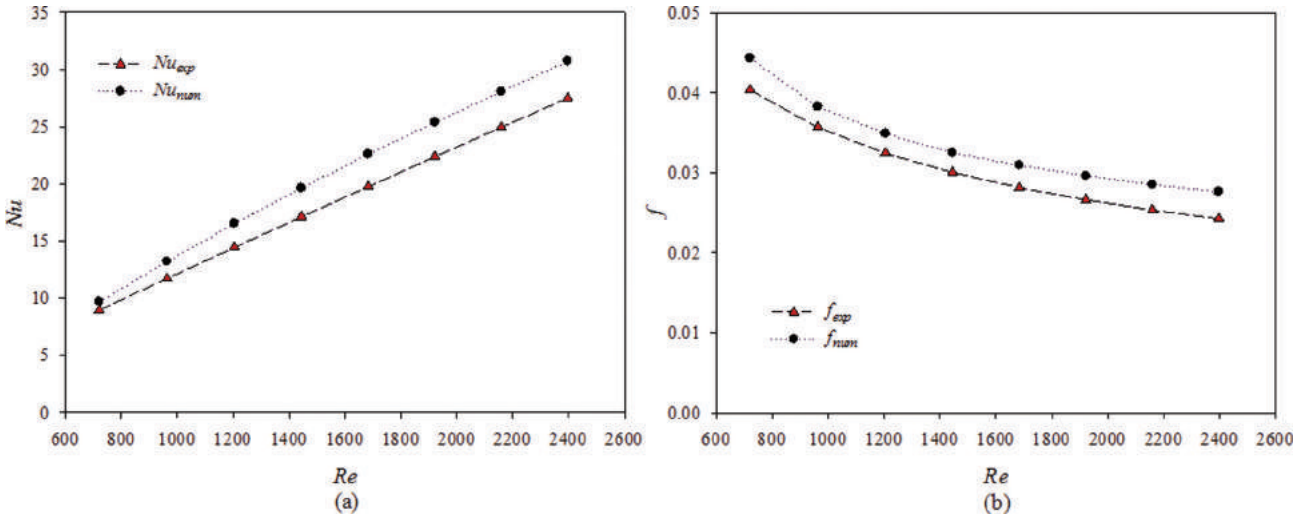

Figure 4. Comparability between experimental and numerical results of **(a)** *Nu* and **(b)** *f*.

results are 14.5% for *Nu* and 13.9% for *f* values, respectively. As a result, the turbulence model that predicts the most accurate results is SST k-ω and has been employed in all analyses.

RESULTS AND DISCUSSION

Thermal-Flow Characteristics

In Fig. 5a, for microchannels with various numbers of VG pairs, the variation of the heat transfer characteristic *j* factors with the angle of attack of VG is shown. The angle of attack has a significant impact on the *j* factor. The *j* factors increase as the angle of attack approaches 90°. The *j* factors begin to fall at the same rate as the angle of attack increases. While the impact of the number of VG pairs is noticeable at angles of attack both smaller and larger than 90°, the impact is significantly diminished at the attack angle of 90°. However, the *j* factors are significantly lower at $a_1=a_2=90°$ when there are 3 VG pairs unlike other angles of attack. VGs positioned at $a_1=a_2=90°$ provide about a 66% increase in heat transfer characteristics for the lowest VG pair number ($N_{VG}=3$). The improvement rate in the *j* factor rises to 76% when $N_{VG}=7$.

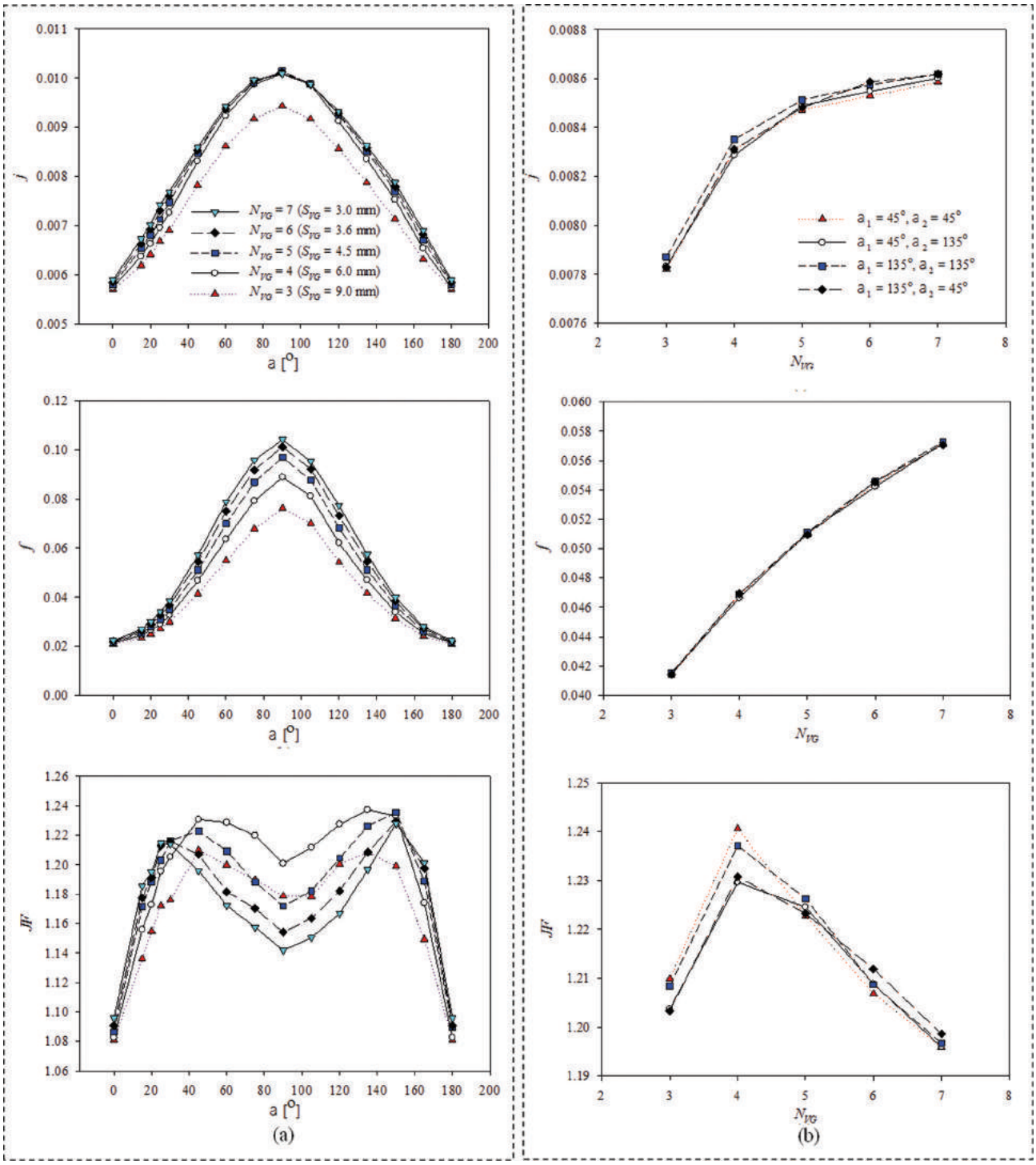

Figure 5. Effects of **(a)** (a_1=a_2=a), **(b)** N_{VG} on j, f and JF (V_f= 5 m/s, L_{VG} = 0.4 mm, W_1 = 0.2 mm).

VGs boost heat transfer, but they also increase pressure losses. The VGs add to the flow's pressure loss because of the local contractions they cause, the energy required to create the vortices, and the rise in friction losses brought on by the vortices' effect on the velocity profile of the flow. In Fig. 5a, the pressure losses caused by the VGs depending on the attack angle are presented as the friction factor f. Friction factors increase until the angle of attack reaches 90°, then decline in conjunction with changes in heat transfer. Increasing the number of VGs in the microchannel increases the f-values significantly. When placed at a 90° angle of attack and N_{VG}=7, the VGs increase the pressure

drop 4.65 times compared to the empty channel. This is a significant increase, far exceeding the augmentation in heat transfer.

The fact that VGs increase both heat transfer and pressure loss suggests that their use may be subject to some restrictions. An increase in pressure loss will result in an increase in pumping power, and also there is a possibility of the formation of local cavitation zones. Nonetheless, the need for cooling in electronic systems necessitates the enhancement of heat transfer. Therefore, the primary objective is to provide the desired heat transfer capacity with as little pressure loss as possible. A criterion is required to evaluate the effectiveness of the employed heat transfer enhancement method. In this study, we have used the *JF* factor to evaluate the enhancement in heat transfer caused by VGs while taking into account pressure loss (Eq. 12). Fig. 6b depicts variations in the *JF* factor based on the angle of attack for a fixed *Re* and the number of different VG pairs. Although the augmentation in heat transfer and the increase in pressure loss have a similar trend depending on the angle of the VG, the amounts of change are quite different. Consequently, the change in *JF* depends on the angle of attack differently than the change in *j* and *f*. The *JF* produces two peaks for all VG pair numbers, indicating that there are two optimal angles of attack for each VG pair. The maximum and minimum *JF* values are obtained with N_{VG} = 4 and 3, respectively. These two microchannels have optimal attack angles of 45° and 135°. 30° and 150° are the optimal angles for N_{VG} = 7 and 6. The optimal angles are 45° and 150° for N_{VG}= 5. For microchannel with N_{VG} = 5 the different optimal attack angles based on the number of VGs are caused by several factors. Changing the number of VGs results in a change in the distance between each VG pair. Therefore, the vortex-vortex interaction and vortex-VG interaction differ. The structure of vortices traveling downstream influences the structure of vortices generated by other VGs.

It is concluded that the number of vortex generator pairs has a significant effect on heat and flow characteristics. For a more in-depth observation of this effect, the *j*, *f*, and *JF* values in Fig. 5b have been utilized depending on the number of VGs. Angles of attack of 45° and 135° are chosen because they produce the best results. Furthermore, the cases where the VG pairs are placed at different angles (a_1 and a_2) are investigated. The *j* factor increases rapidly as the number of VGs increases from 3 to 4, while the rate of increase in *j* decreases as the number of VGs increases further. The number of VGs causes a constant increase in the friction factor *f*. Contrarily, *JF* increases sharply until there are four VG pairs. While N_{VG}=6 and N_{VG}=7 yield the highest *JF* at a_1=135° and a_2=45°, N_{VG}=4 yields the highest *JF* at a_1= a_1=45°. Fig. 6 illustrates how the spacing between the VGs affects the characteristics of pressure loss and heat transfer. A counter-rotating vortex pair is produced by each VG (Fig. 7). The domains of the generated vortex pairs are also affected by the transverse pitch between the VGs. While the W_l/W ratio causes an increase with a little effect on heat transfer, it has less effect on pressure loss. With a rising W_l/W ratio, a gradually declining increase in *JF* is observed (Fig. 6a). As the Reynolds number rises, the intensity of the vortices changes. The interaction between the vortices is altered when the vortex intensity is changed. Therefore, the distance between the VGs to be placed in the microchannel should be taken into account depending on the Reynolds number . However, the optimum N_{VG} remains the same in the current study despite the fact that *j*, *f*, and *JF* decrease with Reynolds numbers (Fig. 6b).

We have stated that the heat transfer and flow characteristic vary based on the structure of the vortices. However, it would be insufficient to reach this conclusion without illustrating the flow structures caused by the vortices. Visualizing the flow structure and heat transfer within the microchannel is an effective method for this purpose. Fig. 7 illustrates streamline results based on VG angles. At a 0° angle of attack, flow separation does not occur as expected, but as the angle of attack increases, flow separation begins to exist around the VGs. Behind each VG, counter-rotating vortex pairs are formed. When the attack angle is 90°, the length of the vortex formation increases rapidly. As the angle of attack of VG exceeds 90°, the vortex formation lengths begin to shorten. The magnitudes of fluid velocity on the streamlines are represented by colors. Especially at the angles of attack close to 90°, significant increases in local flow velocities occur due to the local blocking effect of the microchannel flow cross-section by VGs. This situation increases the fluid mixing and causes the pressure loss to increase considerably. The vortex formation length is highly effective in influencing the characteristic of the flow in the microchannel.

The VG geometry and the angle of attack can be used to control how much the effective vortex zone expands. But this is a limited method when considering the entire microchannel. Therefore, by increasing the number of VGs placed in the microchannel, more heat transfer surfaces can interact with the vortex structures. Fig. 8 presents the variation of streamlines depending on the number of VGs. When we consider the lowest and highest number of VG pairs, it is seen that the vortex formation lengths are shorter than the distance between the VGs. However, these are average values, as the structures formed by the vortex movements that continue periodically throughout the flow dampen each other. An inspection of the instantaneous flow features will show that the vortices are moving downwards. With the increase in the number of VGs, the total number of the swirling flow region within the wakes formed behind the VGs also increases. Flow activities occurring in this region intensify the mixing of cold and hot fluids in the downstream direction, as well as increase the number of pressure loss zones, so they are also very effective on the total

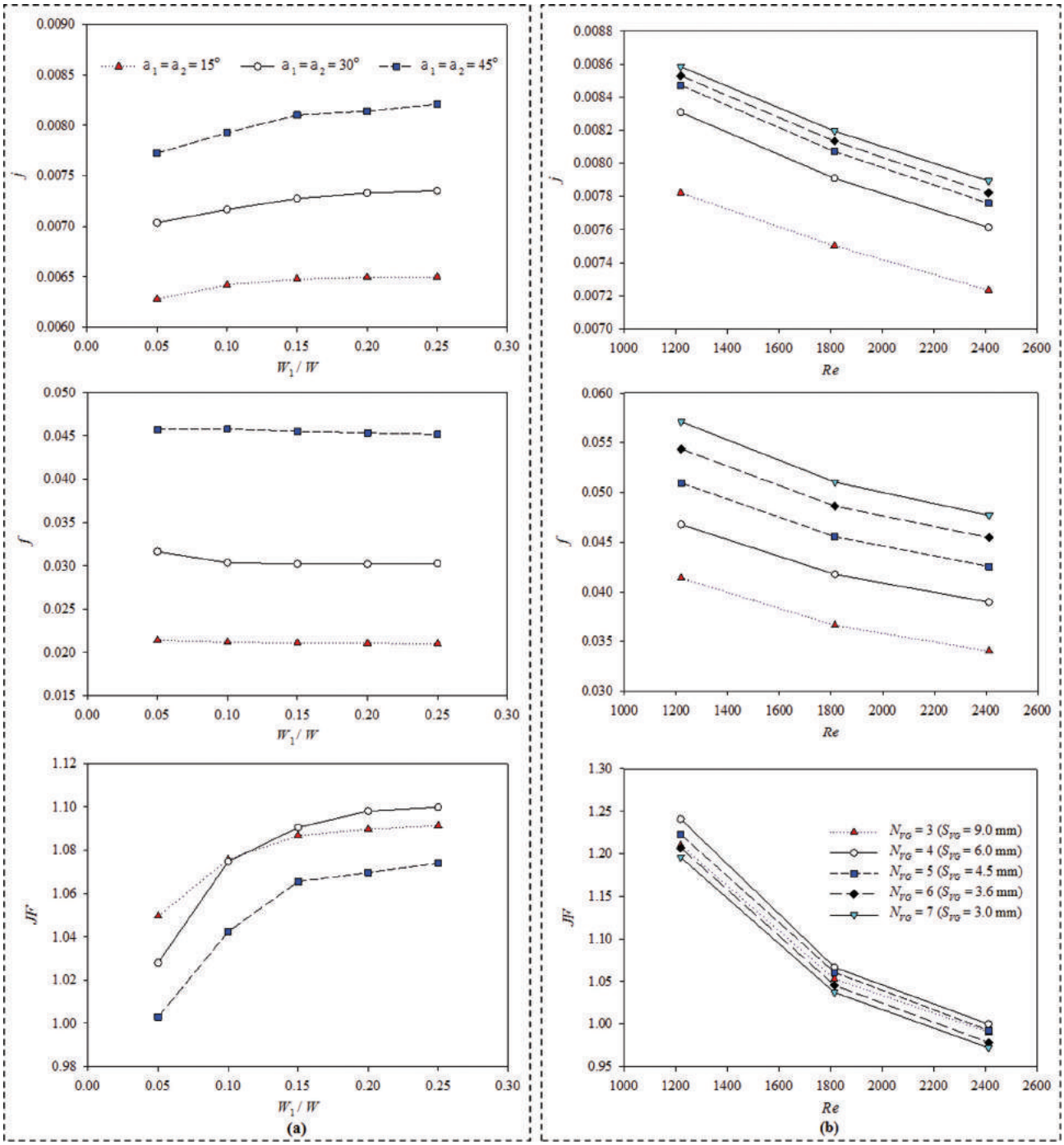

Figure 6. Effects of **(a)** W_1/W ratio (V_f= 7.5 m/s, N_{VG} = 5, L_{VG} = 0.4 mm, α_1= α_2) **(b)** *Re* (V_f= 7.5 m/s, L_{VG}= 0.4 mm, W_1= 0.2 mm, α_1= α_2= 45°) on *j*, *f* and *JF*.

pressure loss. The length of the VG is also highly influential in the formation of vortices. The changes in the flow structure caused by the length of the VGs with 45° attack angles are depicted as streamlines in Fig. 10. Increasing the lengths of the VGs at a constant angle expands the vortex sizes and formation lengths.

Fig. 9a depicts the velocity contours obtained from parallel and perpendicular planes to the flow. The chosen planes contain different regions downstream from the VGs. Low-velocity flow regions are noticeable in the wake region, whereas high-velocity flow regions form close to the leading and trailing edges of the VGs. As the flow moves

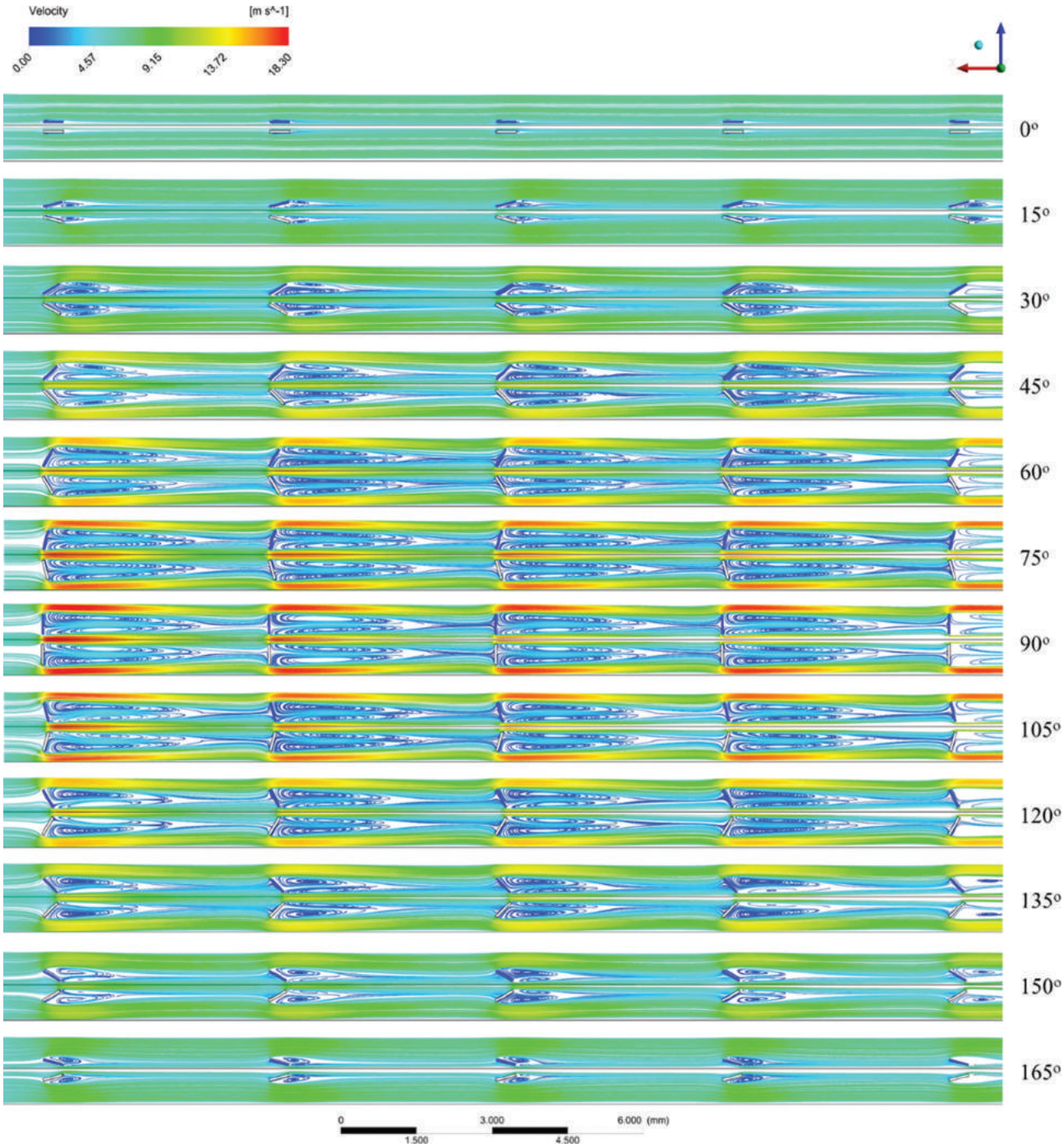

Figure 7. Streamline of different attacks angles (V_f = 5 m/s, N_{VG} = 5, L_{VG} = 0.4 mm, H_{VG} = 0.1 mm, W_1 = 0.2 mm, $\alpha_1 = \alpha_2$ = 45°).

downstream, the velocity differences in the cross-section plane decrease as well. Fig. 9b depicts the temperature contours on the identical planes. In regions of high fluid velocity, the thermal boundary layer is also observed to be thinner. In regions of the wake with low fluid velocity, the thermal boundary layer is thicker. As the downstream flow progresses, the thermal boundary layers in the wake region also begin to thin. Fig. 9c depicts TKE results taken on parallel planes. TKE values are quite high close to the leading and trailing edges, where flow separations and dominant shear layers occur. As the plane moves downstream, the turbulence values first spread over a larger area and then

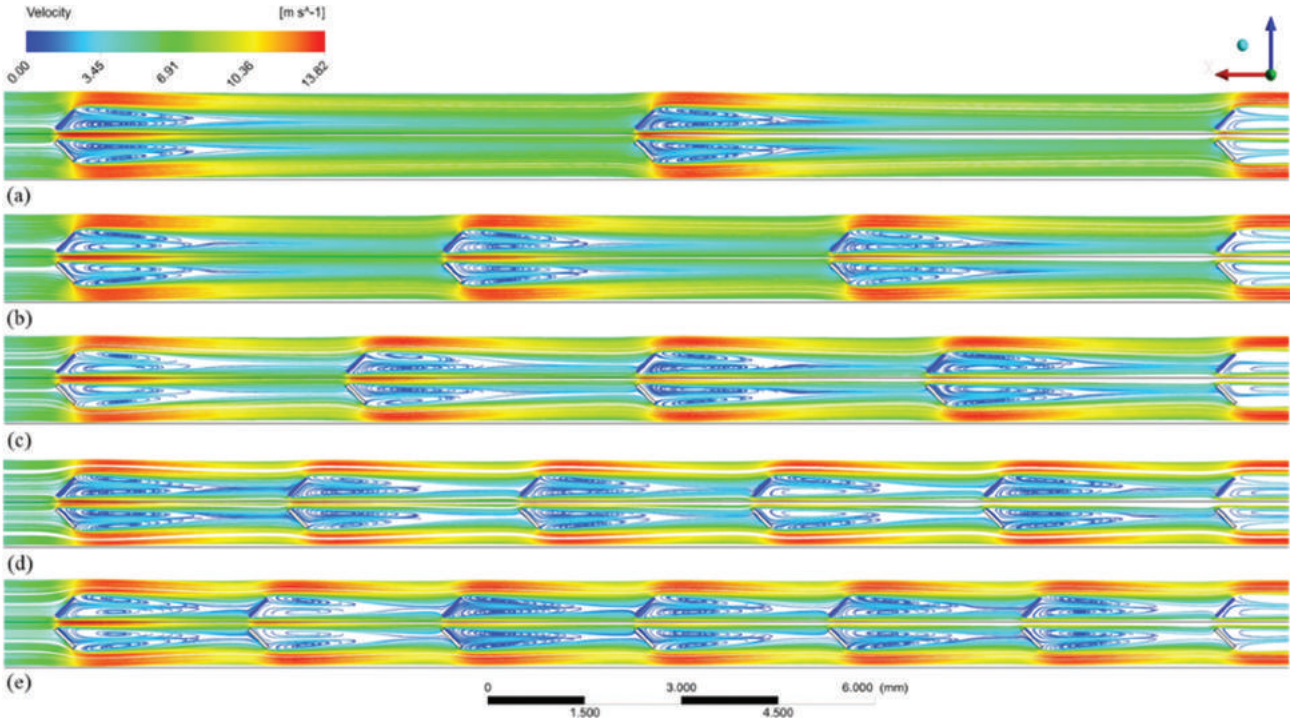

Figure 8. Velocity contours of different number of VG pairs (a) N_{VG} = 3, (b) N_{VG} = 4, (c) N_{VG} = 5, (d) N_{VG} = 6, (e) N_{VG}=7, (V_f = 5 m/s, L_{VG} = 0.4 mm, H_{VG} = 0.1 mm, W_1 = 0.2 mm, α_1 and α_2 = 45°).

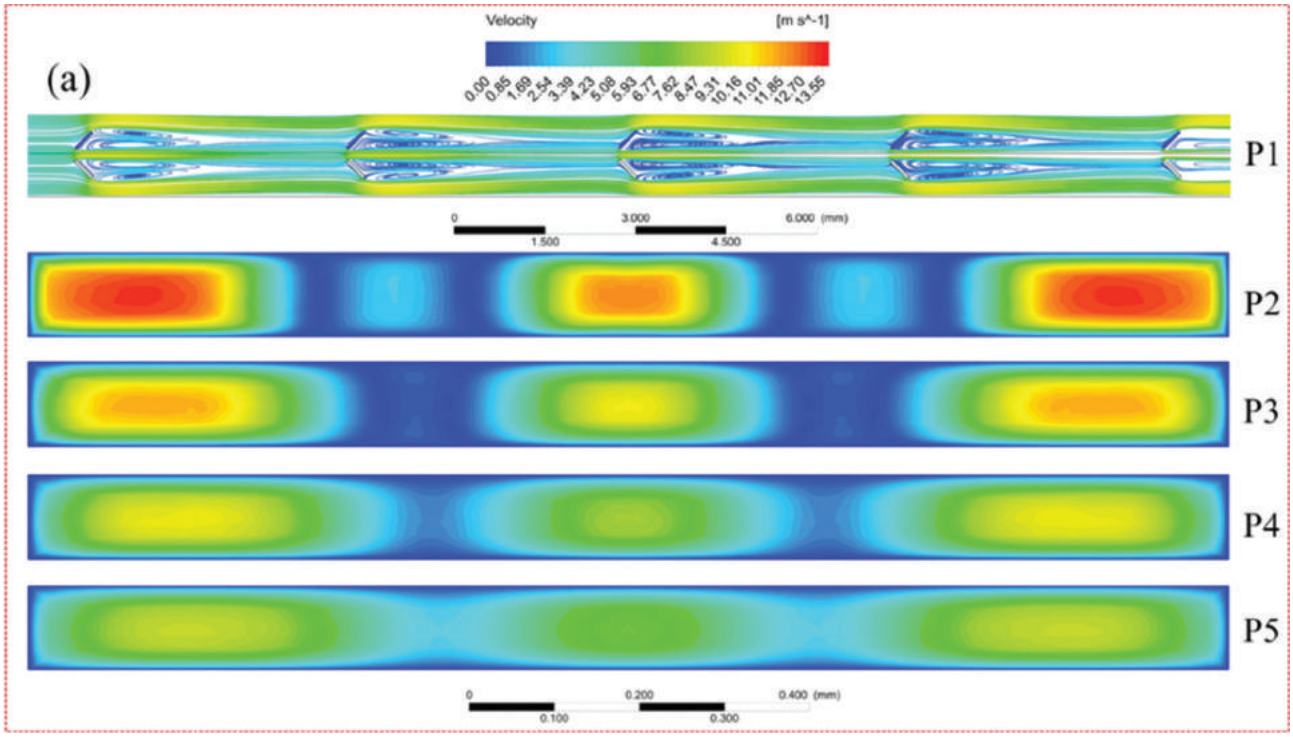

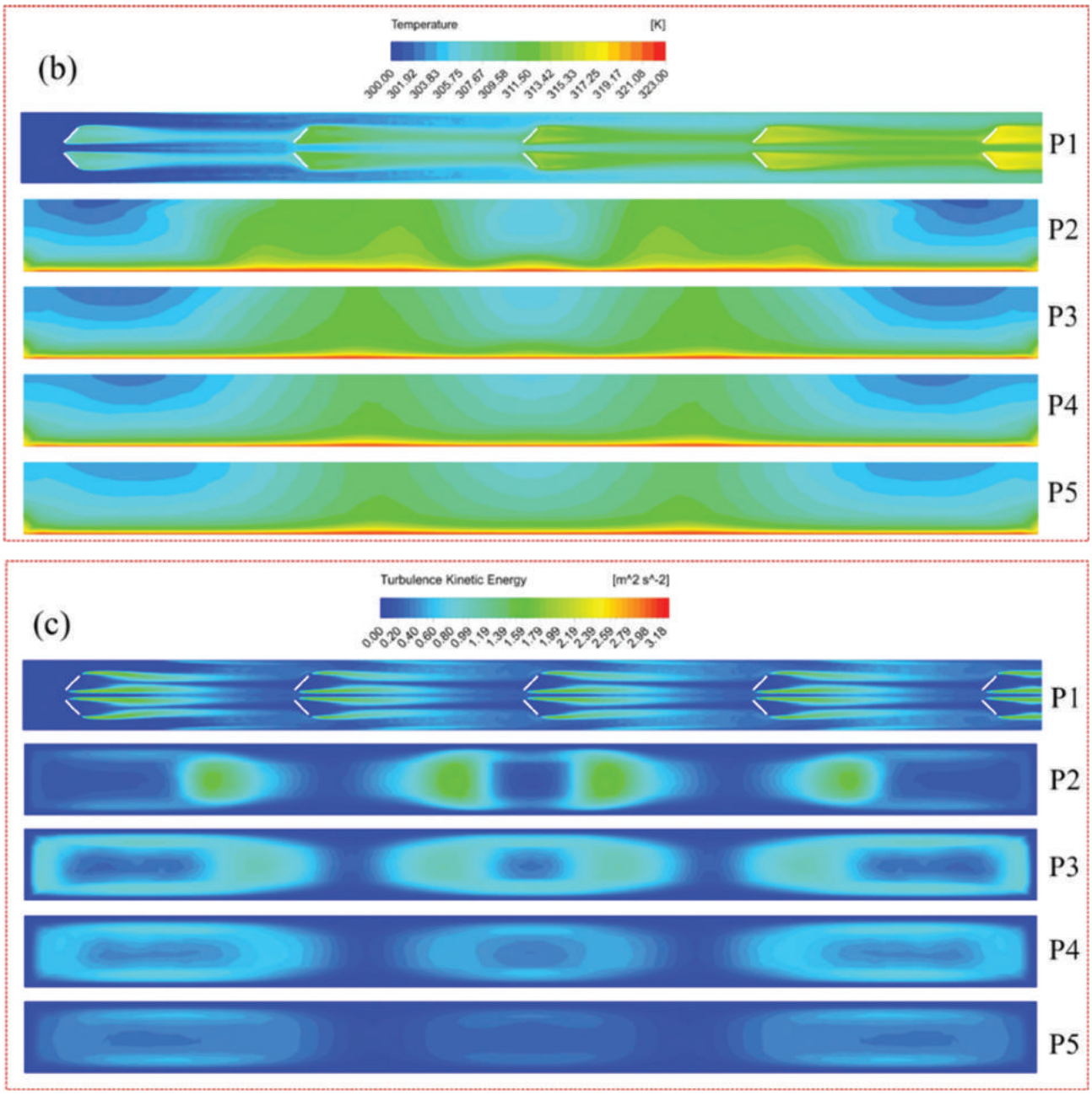

Figure 9. CFD results in different planes (a) velocity contours and streamlines, (b) temperature contours, (c) TKE contours (V_f= 5 m/s, N_{VG}= 5, L_{VG}= 0.4 mm, H_{VG}= 0.1 mm, W_1= 0.2 mm, α_1 and α_2 = 45°).

decrease due to viscous damping. The increase in turbulence value is also one of the factors contributing to the enhancement of heat transfer.

Response Surface Methodology and Sensitivity Analysis

In the current work, the mathematical approach to be employed for compatibility and sensitivity is created by using the Response Surface Method (RSM). Fig. 11 depicts the flowchart of the applied model. This method is applicable to thermal systems including heat exchangers, microchannels, etc. [52,62]. The first phase is the fulfillment of an appropriate DOE approach for mathematical background and sensitivity analysis as illustrated in the flowchart [62]. The primary objective of the DOE is to generate a data set for examining the input-output relationships of design parameters. In this study, we have employed the Latin Hypercube Sampling(LHS)[63] DOE in consideration of the ranges of input parameters provided in Table 1. Since N_{VG} values ranged from 3 to 7 and are constant, the LHS-DOE method is implemented by utilizing different

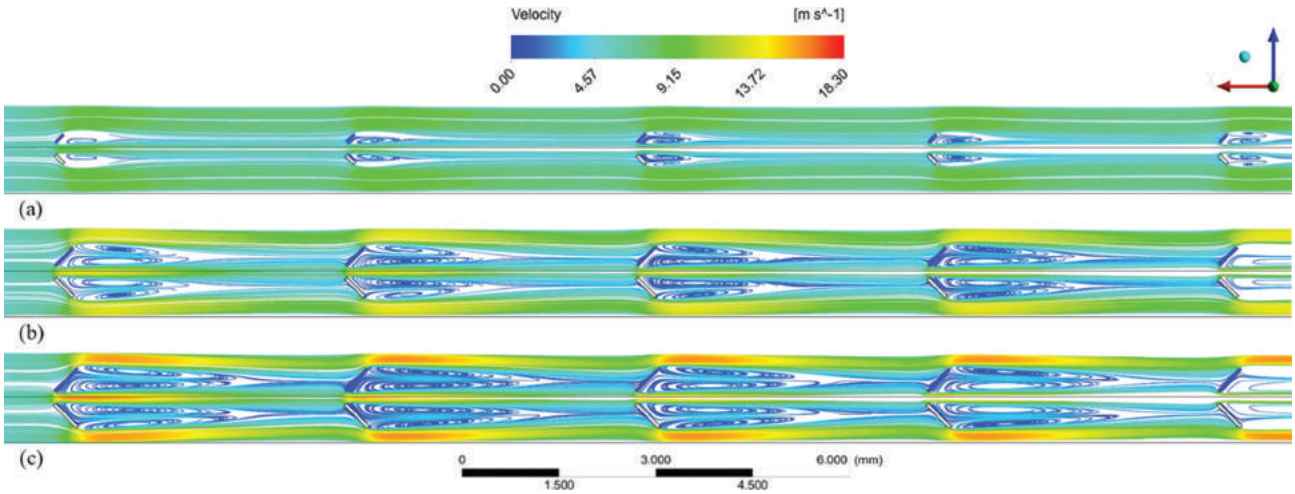

Figure 10. Streamlines for microchannels (a) L_{VG} = 0.175 mm, (b) L_{VG} = 0.3375 mm, (c) L_{VG} = 0.50 mm (V_f = 5 m/s, N_{VG} = 5, H_{VG} = 0.1 mm, W_1 = 0.2 mm, α_1 and α_2 = 45°, Plane 1).

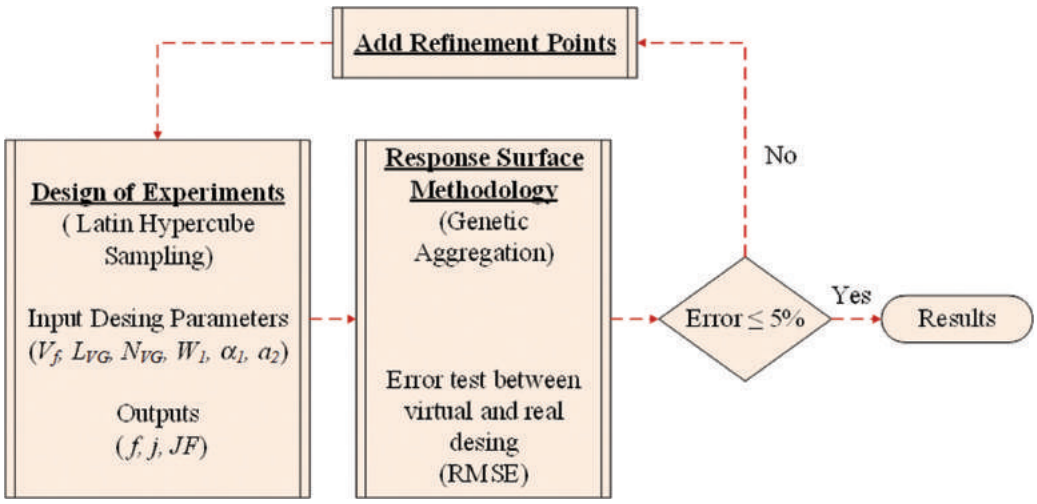

Figure 11. Flow chart of application of Response Surface Methodology.

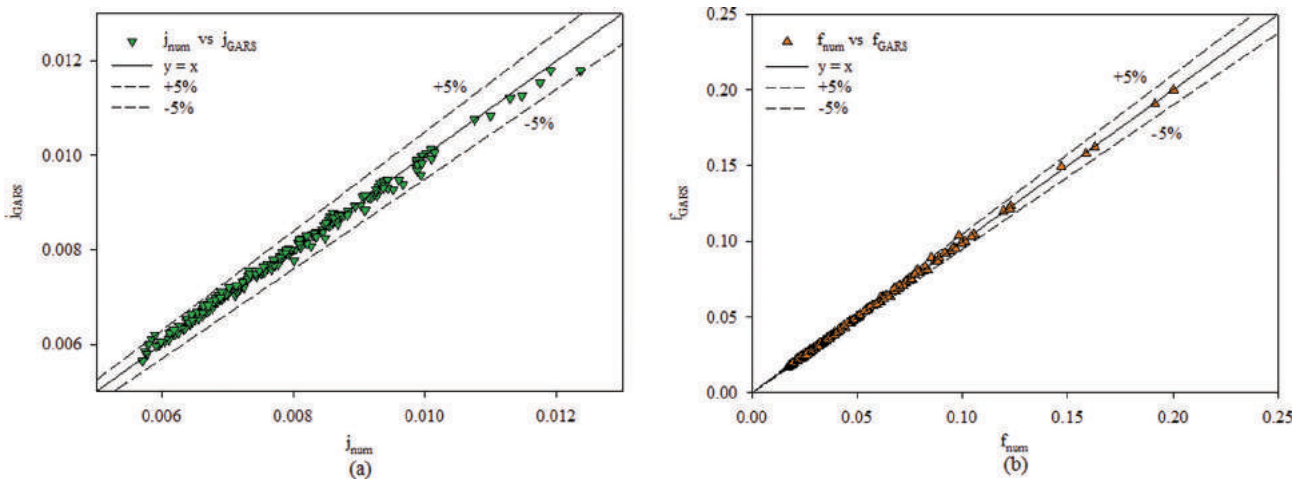

Figure 12. Compatibility between numerical data and GARS results of **(a)** j and **(b)** f.

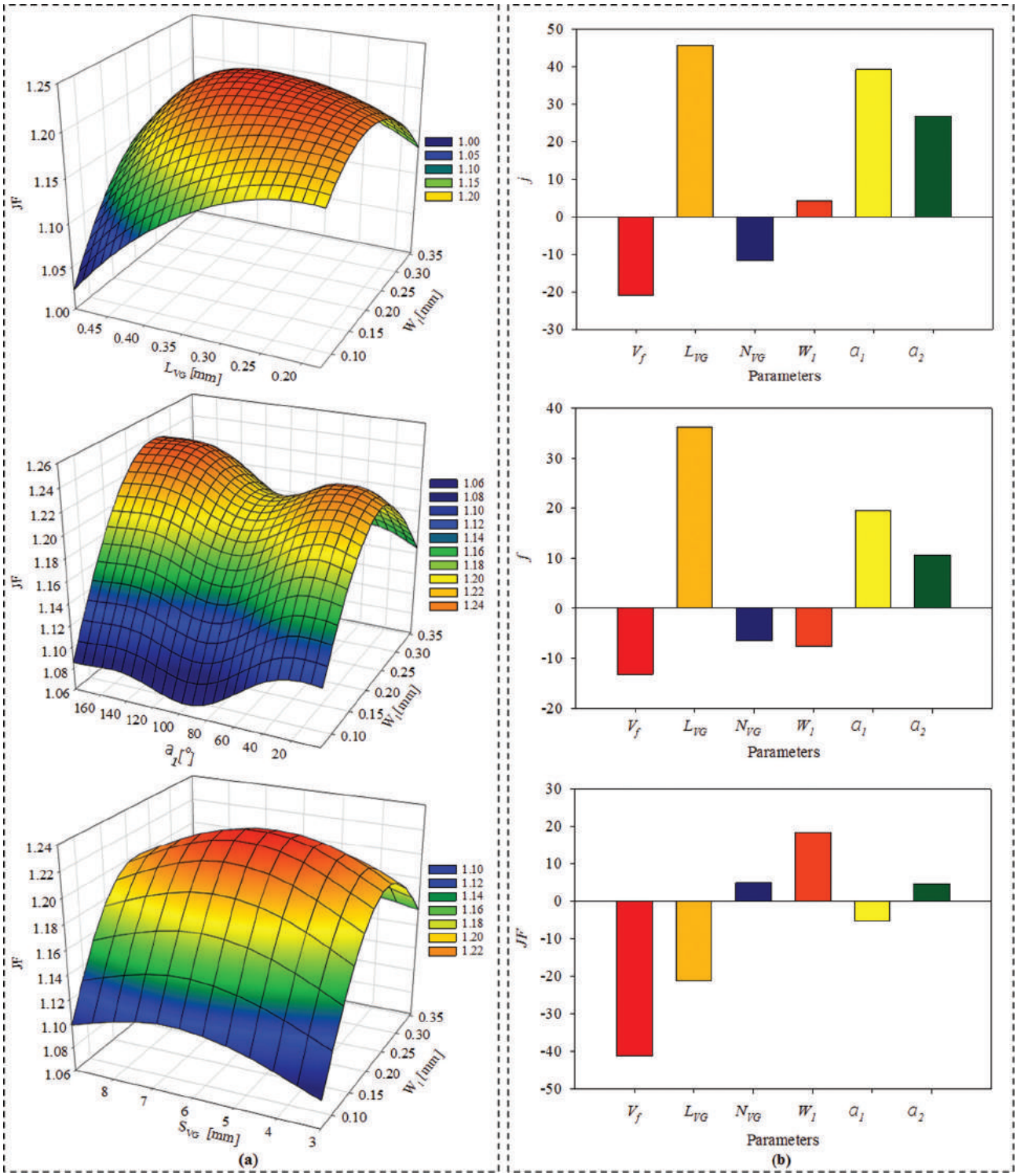

Figure 13. (a) W_1 and L_{VG}, α_1, S_{VG} versus *JF* **(b)** Local Sensitivity Analysis for *j*, *f*, and *JF* (Ref. values V_f= 7.5 m/s, L_{VG}= 0.4 mm, N_{VG}= 5, W_1= 0.2 mm, α_1= α_2= 45°).

input parameters for each N_{VG}. In this case, within the scope of DOE studies, a total of 150 analyses, 30 for each case, have been conducted.

The RSM seems to be a highly effective method for determining the impacts of all parameters on the obtained results. The RSM evaluates not only the individual

interactions between factors, but also their relations with one another. The Genetic Aggregation Response Surface (GARS) technique is considered as the RSM [64]. Due to its capacity to reach multiple response surface solutions and cross-validation, the Genetic Aggregation technique yields more trustworthy results than conventional metamodel [65].

When estimating *j*, *f*, and *JF* values with the GARS method using all the studied parametric and DOE results, the coefficients of determination are reported to be 0.987, 0.989, and 0.953, respectively. Fig.12 demonstrates concurrently the compatibility of *j* and *f* values derived from numerical analysis and the GARS method. Both values can be estimated with a very small margin of error using the GARS method. Both *j* and *f* values produce results within the error margin of ±5%. In this respect, the GARS method is regarded as a highly effective tool for estimating and analyzing the *j* and *f* values in the considered problem.

In Fig.13a, the effects of the changes in W_1 and L_{VG}, α_1, and S_{VG} (N_{VG}) on the *JF* factor are analyzed. In the description of Fig. 13, the reference values of the considered parameters are provided. In general, as depicted in Fig. 13a, the *JF* factor yields the best results at W_1 values in the middle range. On the other hand, it is comprehended that low and high *JF* values produce relatively fewer results. It is observed that increasing the VG generally improves thermal-flow performance. In contrast, the *JF* factor is maximized at the middle values of W_1 and the middle values of L_{VG}. The *JF* factor augments with increasing length at low W_1 intervals, as determined. On the other hand, the *JF* factor reaches its maximum values at W_1 intervals of increasing average length. Increases of up to 25% occur in the relevant intervals. When the effect of the α_1 angle is considered, as depicted in Fig.13a, the change from each W_1 value tends to have roughly similar characteristics. It is observed that the α_1 angle decreases between 75° and 105°. As stated previously, the pressure penalty in this angle range is significantly greater than the heat transfer enhancement, causing this characteristic. The highest enhancement is typically seen between 45° and 135° of α_1. In Fig.13a, the effect of row spacing is taken into account. Examining the figure closely reveals that the average W_1 and S_{VG} values provide the greatest enhancements. In general, according to the results of the GARS method, the *JF* factor varies between 0.78 - 1.38. The maximum value of *JF* factor is obtained for 5 rows of vortex pairs whose L_{VG} = 0.48 mm, W_1 = 0.35 mm, α_1 = 72° and α_2 = 125° and *Re* = 974. The *JF* factor reaches its minimum value of 0.78 under conditions of *Re* = 2282, N_{VG} = 7, L_{VG} = 0.50 mm, W_1 = 0.32 mm, α_1 = 97°, and α_2=95°. Similarly, the enhancement in heat transfer compared to the empty channel ranges from 6% to 230%. The maximum increase in Colburn - *j* factor occurs for *Re* = 969 and microchannel properties of N_{VG} = 7, L_{VG}=0.45 mm, W_1=0.14 mm, α_1=92°, α_2=120°. The corresponding increase in the friction factor *f* is 950%. It is observed that the pressure loss changes in terms of friction factor *f* in the range of 5% to 1466% compared to the empty channel. In the results obtained by the GARS method, when α_1 and α_2 values are 0°, the values of *j* and *f* are dominantly the minimum regardless of the dimensions of the other parameters. The relevant results are also in excellent agreement with the numerical study results.

According to the results of the GARS method, local sensitivity analysis has been also applied within the scope of the study. Local sensitivity study concentrates on the sensitivity around a set of parameters and examines the local effect of variation in input factors on model response. Such sensitivity is frequently evaluated at these factor values using gradients or partial derivatives of the output functions, which means that when evaluating the local sensitivity of one input factor, the values of the other input factors are held constant. In the context of the research, sensitivity analysis has been performed to investigate the impact of five different geometrical parameters (L_{VG}, N_{VG}, W_1, α_1, α_2), in addition to incoming velocity, on *j*, *f*, and *JF* (Fig. 13b). In general, it is comprehended that each factor has a substantial impact on the relevant outputs. However, it appears that the effects of W_1 and N_{VG} on the Colburn-*j* factor are minimal. The sensitivity analysis for *f* yields comparable results. All three output values are determined to decrease as the velocity increases. L_{VG} is a crucial input variable and parameter for both pressure drop and heat transfer. It is evident that the difference between the smallest and largest values influences more than 30% of the three outputs. Compared to other parameters, the number of rows has a relatively minor impact on the outputs. The effect of N_{VG} on *j* is approximately 15%, while its effect on *f* and *JF* is approximately 10%. Observably, the angle of attack has a significant effect on *j* and *f*. However, its effect on *JF* decreases. Taking into account the smallest and largest values of the effects of W_1 value on *JF*, a result change of up to 20% is recognized.

CONCLUSION

In the current study, we have aimed to increase the heat transfer capacity of a microchannel equipped with vortex generators (VGs). For this, we have decorated the microchannel with rectangular VGs of different sizes, numbers, and angles of attack for heat transfer enhancement and used CFD to predict the flow structure and heat transfer. While evaluating the heat transfer and pressure loss characteristics as Colburn-*j* factor, friction factor *f* and JF factor, we have used streamline, velocity, temperature, and TKE contours to understand the effects of VGs on flow and heat transfer structure. We have performed the Genetic Aggregation Response Surface (GARS) methodology to find the optimum design for VGs by considering heat transfer and pressure loss, and to define the effect of design parameters on the results. The most essential findings of the study are as follows:

- Heat transfer is significantly enhanced by the fluid mixing produced by swirling flow of vortices. A rise in the fluid mixing is ensured by secondary flow structures, which transfer the hot fluid on the hot surface to the main flow region and the cold fluid from the main flow region to the cold surfaces.
- As VG attack angles and lengths increase, the vortex formation lengths increases, and the heat transfer and pressure losses are highly dependent on the vortex formation length. Colburn-*j* factor increases with the thinning of the thermal boundary layer.
- Colburn-*j* factor increases considerably, especially at the 90° angle of attack. However, since the pressure losses also increase in this case, the *JF* factor, performance evaluation criterion, takes maximum values at the attack angles range of 30°-45° and 135°-150° of depending on the number of VG rows.
- The compatibility of less than 5% is discovered between the numerical analysis results and the GARS Methodology.
- According to the GARS technique, the highest value of the *JF* factor is around 1.38 in the channel with *Re* = 974, N_{VG} = 5, L_{VG} = 0.48 mm, W_1 = 0.35 mm, α_1 = 72°, α_2 = 125°.
- The highest augmentation in *j* factor is around 270% in the case of *Re* = 2287 and microchannel specifications N_{VG} = 7, L_{VG}=0.45 mm, W_1=0.14 mm, α_1=92°, α_2=120°, while the corresponding increase in *f* friction factor is 950% when compared to the empty channel.
- It has been determined that both *j* and *f* values generally present minimum results for α_1 and α_2 = 0°.
- The GARS technique is employed for sensitivity analysis, and it is comprehended that all input parameters considered have a significant impact on *j*, *f,* and *JF*. Furthermore, the sensitivity analysis reveals that L_{VG} has the greatest impact on *j* and *f* values, whereas V_f is the most influential parameter on *JF*.

We believe our research will shed light on efforts to improve heat transfer in microchannels. Despite the fact that we have carefully considered many parameters, it is always possible to design higher-performance microchannels. It may be possible to manufacture microchannels with much higher heat transfer capacity by using different types of VG geometries, changing the microchannel structure, and combining more than one flow control method (active or passive).

NOMENCLATURE

A	Area, m^2
A_c	Channel cross-section area, m^2
A_h	Heated surface area (base area), m^2
C_p	Specific heat coefficient of fluid, $J.kg^{-2}.K^{-1}$
D_h	Hydraulic diameter, m
f	Friction factor [-]
H	Channel height [m]
h	Heat convection coefficient, $W.m^{-2}.K^{-1}$
k	Turbulent kinetic energy, $J.kg^{-1}$
L	Channel length, m
Nu	Average Nusselt number [-]
N	Number of VG pairs
j	Colburn-j factor [-]
JF	Thermal & hydraulic performance criteria [-]
p	Pressure, Pa
P_w	Channel wetted perimeter, m
Pr	Prandtl number [-]
$\dot{Q}$	Heat transfer rate, W
Re	Reynolds number [-]
S	The longitudinal pitch between VG pairs, mm
T_h	Heated surface temperature, °C
T_i	Fluid inlet temperature, °C
T_o	Fluid outlet temperature, °C
u	Velocity component, $m\ s^{-1}$
u'	Fluctuating velocity component, $m\ s^{-1}$
V_f	Incoming fluid velocity, $m.s^{-1}$
W	Channel width, m
W_1	The traverse pitch between VG pairs, mm
x	Coordinate
ΔT_m	Logarithmic mean temperature difference, °C
ΔP	Pressure drop, Pa

Greek symbols

α	Angle of attack, °
Δ	Difference
δ_{ij}	Knocker delta
λ	Thermal conductivity, $W\ m^{-1}\ °C^{-1}$
ω	The specific dissipation, $1.s^{-1}$
μ	Dynamic Viscosity, Pa.s
ν	Kinematic viscosity, $m^2\ s^{-1}$, $= \mu\ \rho^{-1}$
ρ	Density, $kg.m^{-3}$

Subscripts

f	Fluid
eff	Effective
h	Heated surface
i	Inlet
i, j, k	Direction of coordinate
o	Outlet
0	Empty channel (without VGs)
exp	Experimental studies
num	Numerical studies
$GARS$	Data from GARS studies
s	Solid
t	Turbulent
VG	Vortex generator

AUTHORSHIP CONTRIBUTIONS

Authors equally contributed to this work.

DATA AVAILABILITY STATEMENT

The authors confirm that the data that supports the findings of this study are available within the article. Raw data that support the finding of this study are available from the corresponding author, upon reasonable request.

CONFLICT OF INTEREST

The author declared no potential conflicts of interest with respect to the research, authorship, and/or publication of this article.

ETHICS

There are no ethical issues with the publication of this manuscript.

REFERENCES

[1] Tuckerman DB, Pease RFW. High-Performance Heat Sinking for VLSI. IEEE Electron Device Lett 1981;2:126–129. [CrossRef]

[2] Xu B, Ooi KT, Wong NT, Choi WK. Experimental investigation of flow friction for liquid flow in microchannels. Int Commun Heat Mass Transf 2000;27:1165–1176. [CrossRef]

[3] Wang BX, Peterson GP. Frictional flow characteristics of water flowing through rectangular microchannels. Exp Heat Transf 1994;7:249–264. [CrossRef]

[4] Wang BX, Peterson GP. Heat transfer characteristics of water flowing through microchannels. Exp Heat Transf 1994;7:265–283. [CrossRef]

[5] Peng XF, Peterson GP. Convective heat transfer and flow friction for water flow in microchannel structures. Int J Heat Mass Transf. 1996;39:2599–2608. [CrossRef]

[6] Peng XF, Peterson GP. The effect of thermofluid and geometrical parameters on convection of liquids through rectangular microchannels. Int J Heat Mass Transf 1995;1395:755–758. [CrossRef]

[7] Peng XF, Peterson GP. Forced convection heat transfer of single-phase binary mixtures through microchannels. Exp Therm Fluid Sci 1996;12:98–104. [CrossRef]

[8] Morini GL. Single-phase convective heat transfer in microchannels: A review of experimental results. Int J Therm Sci 2004;43:631–651. [CrossRef]

[9] Colgan EG, Furman B, Gaynes M, Graham WS, LaBianca NC, Magerlein JH, et al. A practical implementation of silicon microchannel coolers for high power chips. IEEE Trans Components Packag Technol 2007;30:218–225. [CrossRef]

[10] Morini GL, Yang Y, Lorenzini M. Experimental analysis of gas micro-convection through commercial microtubes. Exp Heat Transf 2012;25:151–171. [CrossRef]

[11] Özdemir MR, Sözbir R, Yilmaz M. Exergo-economic analysis of microchannels in single-phase flow. J Therm Eng 2018;4:2371–2380. [CrossRef]

[12] Nakharintr L, Naphon P, Wiriyasart S. Effect of jet-plate spacing to jet diameter ratios on nanofluids heat transfer in a mini-channel heat sink. Int J Heat Mass Transf 2018;116:352–361. [CrossRef]

[13] Ambatipudi KK, Rahman MM. Analysis of conjugate heat transfer in microchannel heat sinks. Numer Heat Transf Part A Appl 2000;37:711–731. [CrossRef]

[14] Zhao CY, Lu TJ. Analysis of microchannel heat sinks for electronics cooling. Int J Heat Mass Transf 2002;45:4857–4869. [CrossRef]

[15] Belhadj A, Bouchenafa R, Saim R. Numerical investigation of forced convection of nanofluid in microchannels heat sinks. J Therm Eng 2018;4:2263–2273. [CrossRef]

[16] Madani K, Maad R Ben, Abidi-Saad A. Numerical investigation of cooling a ribbed microchannel using nanofluid. J Therm Eng 2018;4:2408–2422. [CrossRef]

[17] Gaikwad VP, Mohite SS, Shinde SS, Dherange ML. Enhancement in thermo-hydraulic performance of microchannel heat sink with secondary flows of leaf venation pattern. J Therm Eng 2020;6:677–696. [CrossRef]

[18] Meral ZK, Parlak N. Experimental research and cfd simulation of cross flow microchannel heat exchanger. J Therm Eng 2021;7:270–283. [CrossRef]

[19] Gaikwad VP, Mohite SS. Performance analysis of microchannel heat sink with flow disrupting pins. J Therm Eng 2022;8:402–425. [CrossRef]

[20] Toh KC, Chen XY, Chai JC. Numerical computation of fluid flow and heat transfer in microchannels. Int J Heat Mass Transf. 2002;45:S133–S141. [CrossRef]

[21] Gönül A, Çolak AB, Kayaci N, Okbaz A, Dalkilic AS. Prediction of heat transfer characteristics in a microchannel with vortex generators by machine learning. Kerntechnik. 2023. doi: 10.1515/kern-2022-0075. [E pub ahead of print]. [CrossRef]

[22] Chai L, Xia G, Wang L, Zhou M, Cui Z. Heat transfer enhancement in microchannel heat sinks with periodic expansion-constriction cross-sections. Int J Heat Mass Transf 2013;62:741–751. [CrossRef]

[23] Kuppusamy NR, Mohammed HA, Lim CW. Numerical investigation of trapezoidal grooved microchannel heat sink using nanofluids. Thermochim Acta. 2013;573:39–56. [CrossRef]

[24] Wang XD, Bin An, Xu JL. Optimal geometric structure for nanofluid-cooled microchannel heat sink under various constraint conditions. Energy Convers Manag 2013;65:528–538. [CrossRef]

[25] Lin L, Chen YY, Zhang XX, Wang XD. Optimization of geometry and flow rate distribution for double-layer microchannel heat sink. Int J Therm Sci 2014;78:158–168. [CrossRef]
[26] Leng C, Wang XD, Wang TH. An improved design of double-layered microchannel heat sink with truncated top channels. Appl Therm Eng 2015;79:54–62. [CrossRef]
[27] Lin L, Zhao J, Lu G, Wang XD, Yan WM. Heat transfer enhancement in microchannel heat sink by wavy channel with changing wavelength/amplitude. Int J Therm Sci 2017;118:423–434. [CrossRef]
[28] Sun L, Li J, Xu H, Ma J, Peng H. Numerical study on heat transfer and flow characteristics of novel microchannel heat sinks. Int J Therm Sci 2022;176:107535. [CrossRef]
[29] Belhadj A, Bouchenafa R, Saim R. A numerical study of forced convective flow in microchannels heat sinks with periodic expansion-constriction cross section. J Therm Eng 2018;4:1912–1925. [CrossRef]
[30] Ramesh KN, Sharma TK, Rao GAP. Latest Advancements in Heat Transfer Enhancement in the Micro-channel Heat Sinks: A Review. Springer Netherlands; 2021. [CrossRef]
[31] Dewan A, Srivastava P. A review of heat transfer enhancement through flow disruption in a microchannel. J Therm Sci. 2015;24:203–214. [CrossRef]
[32] Sidik NAC, Muhamad MNAW, Japar WMAA, Rasid ZA. An overview of passive techniques for heat transfer augmentation in microchannel heat sink. Int Commun Heat Mass Transf 2017;88:74–83. [CrossRef]
[33] Yang JS, Lee DW, Choi GM. Numerical investigation of fluid flow and heat transfer characteristics by common-flow-up. Int J Heat Mass Transf. 2008;51:6332–6336. [CrossRef]
[34] Hiravennavar SR, Tulapurkara EG, Biswas G. A note on the flow and heat transfer enhancement in a channel with built-in winglet pair. Int J Heat Fluid Flow 2007;28:299–305. [CrossRef]
[35] Wang Q, Chen Q, Wang L, Zeng M, Huang Y, Xiao Z. Experimental study of heat transfer enhancement in narrow rectangular channel with longitudinal vortex generators. Nucl Eng Des 2007;237:686–93. [CrossRef]
[36] Yang JS, Lee DW, Choi GM. Numerical investigation of fluid flow and heat transfer characteristics by common-flow-up. Int J Heat Mass Transf 2008;51:6332–6336. [CrossRef]
[37] Khanjian A, Habchi C, Russeil S, Bougeard D, Lemenand T. Effect of rectangular winglet pair roll angle on the heat transfer enhancement in laminar channel flow. Int J Therm Sci 2017;114:1–14. [CrossRef]
[38] Mundhe SV, Bindu RS. Numerical and experimental investigations on performance evaluation of a conical offset vortex generator inserts to improve convective heat transfer coefficient. J Therm Eng 2020;6:858–872. [CrossRef]
[39] Al-Dulaimi MJ, Kareem FA, Hamad FA. Numerical investigation of the heat transfer enhancement inside a square duct with rectangular vortex generators. J Therm Eng 2022;8:1–13. [CrossRef]
[40] Hu D, Zhang Q, Song K, Gao C, Zhang K, Su M, et al. Performance optimization of a wavy finned-tube heat exchanger with staggered curved vortex generators. Int J Therm Sci 2023;183:107830. [CrossRef]
[41] Xie C, Yan G, Ma Q, Elmasry Y. Flow and heat transfer optimization of a fin-tube heat exchanger with vortex generators using Response Surface Methodology and Artificial Neural Network. Case Stud Therm Eng 2022;39:102445. [CrossRef]
[42] Song K, Hu D, Zhang Q, Zhang K, Wu X, Wang L. Thermal-hydraulic characteristic of a novel wavy fin-and-circle tube heat exchanger with concave curved vortex generators. Int J Heat Mass Transf 2022;194:123023. [CrossRef]
[43] Sharma B, Bhushan G, Sachdeva G. Effect of flow structure on heat transfer in compact heat exchanger by using finite thickness winglet at acute angle. J Therm Eng 2017;3:1149–1162. [CrossRef]
[44] Çelik HS, Erbay B. Heat transfer enhancement using different types of turbulators on the heat exchangers. J Therm Eng 2021;7:1654–1670. [CrossRef]
[45] Fiebig M, Brockmeier U, Mitra NK, Göhler T. Structure of velocity and temperature fields in laminar channel flows with longitudinal vortex generators. Numer Heat Transf Part A 1989;15:281–302. [CrossRef]
[46] Luo C, Wu S, Song K, Hua L, Wang L. Thermo-hydraulic performance optimization of wavy fin heat exchanger by combining delta winglet vortex generators. Appl Therm Eng 2019;163:114343. [CrossRef]
[47] Ryu K, Yook SJ, Lee KS. Optimal design of a corrugated louvered fin. Appl Therm Eng 2014;68:76–79. [CrossRef]
[48] Okbaz A, Pınarbaşı A, Olcay AB. Experimental investigation of effect of different tube row-numbers, fin pitches and operating conditions on thermal and hydraulic performances of louvered and wavy finned heat exchangers. Int J Therm Sci 2020;151:106256. [CrossRef]
[49] Okbaz A, Pınarbaşı A, Olcay AB, Hilmi Aksoy M. An experimental, computational and flow visualization study on the air-side thermal and hydraulic performance of louvered fin and round tube heat exchangers. Int J Heat Mass Transf 2018;121:153–169. [CrossRef]
[50] Okbaz A, Olcay AB, Cellek MS, Pinarbasi A. Computational investigation of heat transfer and pressure drop in a typical louver fin-and-tube heat

exchanger for various louver angles and fin pitches. EPJ Web Conf 2017;143:02084.

[51] Okbaz A, Pinarbasi A, Olcay AB. 3D computational analysis of thermal and hydraulic performance of louvered fin heat exchanger with variable louver angle and louver pitch. Proc ASME Int Mech Eng Congr Expo. 2016;6B:V06BT08A025. [CrossRef]

[52] Gönül A, Okbaz A, Kayaci N, Selim Dalkilic A. Flow optimization in a microchannel with vortex generators using genetic algorithm. Appl Therm Eng 2022;201:117738. [CrossRef]

[53] Liu C, Teng JT, Chu JC, Chiu YL, Huang S, Jin S, et al. Experimental investigations on liquid flow and heat transfer in rectangular microchannel with longitudinal vortex generators. Int J Heat Mass Transf. 2011;54:3069–3080. [CrossRef]

[54] Chen C, Teng JT, Cheng CH, Jin S, Huang S, Liu C, et al. A study on fluid flow and heat transfer in rectangular microchannels with various longitudinal vortex generators. Int J Heat Mass Transf 2014;69:203–214. [CrossRef]

[55] Ebrahimi A, Roohi E, Kheradmand S. Numerical study of liquid flow and heat transfer in rectangular microchannel with longitudinal vortex generators. Appl Therm Eng 2015;78:576–583. [CrossRef]

[56] Hsiao KY, Wu CY, Huang YT. Fluid mixing in a microchannel with longitudinal vortex generators. Chem Eng J 2014;235:27–36. [CrossRef]

[57] Al-Asadi MT, Alkasmoul FS, Wilson MCT. Heat transfer enhancement in a micro-channel cooling system using cylindrical vortex generators. Int Commun Heat Mass Transf 2016;74:40–47. [CrossRef]

[58] Glassbrenner CJ, Slack GA. Thermal conductivity of silicon and germanium from 3°K to the melting point. Phys Rev 1964;134: A1058. [CrossRef]

[59] Wagner W, Kruse A. Properties of Water and Steam / Zustandsgrößen von Wasser und Wasserdampf. Berlin: Springer; 1998.

[60] ANSYS Inc. ANSYS Fluent Theory Guide. Release 19.1. Canonsburg (PA): ANSYS Inc.; 2017.

[61] Kirkar SM, Gönül A, Celen A, Dalkilic AS. Multi-Objective Optimization of Single-Phase Flow Heat Transfer Characteristics in Corrugated Tubes. Int J Therm Sci 2023;186:108119. [CrossRef]

[62] Gönül A, Ağra Ö. Investigation of heat transfer in tandem and staggered arrangement of wires on single layer wire-on-tube condensers in cross-flow. Int J Heat Mass Transf 2020;158:119923. [CrossRef]

[63] McKay MD, Beckman RJ, Conover WJ. A comparison of three methods for selecting values of input variables in the analysis of output from a computer code. Technometrics 1979;21:239–245. [CrossRef]

[64] ANSYS Inc. ANSYS DesignXplorer User's Guide. Release 14.0. Canonsburg (PA): ANSYS Inc.; 2011.